Springer

Journal of Mechanical Science and Technology 23 (2009) 2565~2573

Journal of Mechanical Science and Technology

www.springerlink.com/content/1738-494x
DOI 10.1007/s12206-009-0706-8

Analysis of spatial vapor-phase distribution using the LIF method on multi-component fuel †

J. K. Yoon[1], K. J. Myong[2,*], J. Senda[3] and H. Fujimoto[3]

[1]*Department of Mechanical & Automotive Engineering, Kyungwon University, Seongnam, Gyeonggi, 461-701, Korea*
[2]*Department of Automobiles, Chosun College of Science & Technology, Gwangju 501-744, Korea*
[3]*Department of Mechanical Engineering, Doshisha University, 1-3, Miyakodani, Tatara, Kyotanabe, Kyoto 610-0321, Japan*

(Manuscript Received January 19, 2009; Revised April 27, 2009; Accepted June 18, 2009)

Abstract

We analyzed the vapor-phase distribution and behavior of each component in multi-component fuel (MCF). Evaporation characteristic of MCF was researched by laser-induced fluorescent (LIF) method. A pulsed Nd-YAG laser was used as incident light, and an experiment was performed in a constant-volume vessel so that optical measurement could be possible. MCF was injected through electronically controlled common rail injector into the vessel. I-octane (C_8H_{18}), n-dodecane ($C_{12}H_{26}$) and n-hexadecane ($C_{16}H_{34}$) were selected to be low boiling point (LO-B.P.), mid boiling point (MI-B.P.) and high boiling point (HI-B.P.) components, respectively, and Fuel *A*, Fuel *B* and Fuel *C*, made by compounding those components at different mass fractions, were used as MCF. Experimentation was performed under the conditions that injection pressures were 42MPa, 72MPa and 112MPa, respectively, ambient gas density was 15kg/m^3 and ambient gas temperature was 700K. The spatial vapor-phase distribution, dispersion process of mixture, and vapor-phase homogeneity were researched. It was ascertained that the vapor-phase of MCF showed stratified distribution and the dispersion of mixture was improved in proportion to the mass fraction of the LO-B.P. component.

Keywords: Vapor phase distribution; Multi-component fuel; LIF (Laser-Induced Fluorescence); LO-B.P. (Low-Boiling Point)

1. Introduction

Various studies have been carried out relating to liquid- and vapor-phase behavior of diesel spray, as those exert influence on the characteristics of combustion and exhaust gas emission. In experimental studies, the vapor-phase characteristic has been researched to quantify vapor-phase distribution by using two-dimensional LIF or Exciplex [1]; the vapor-phase behavior of each component in MCF spray has hardly been studied. MCF spray has been actively studied in the sphere of numerical analysis, and Abraham et al. [2] presumed that the vapor-phase distribution of each component in MCF may be stratified due to different properties.

Fig.1 shows a distillation curve of each component in MCF [3, 4], that is, the distillation curve of i-octane (C_8H_{18}) and n-hexadecane ($C_{12}H_{26}$) in MCF, on conditions that the two were compounded at the mass fraction of 6:3:1 (Fuel *A*) and 1:3:6 (Fuel *C*), respectively. In the case of Fuel *A*, each component rapidly began to be distilled due to the abundant LO-B.P. component (i-octane). On the other hand, in the case of Fuel *C*, each component is slow in distilling. Vapor-phase characteristic of MCF spray is different according to compound component and that fuel property.

2. Experimental description

2.1 Constant-volume vessel

Fig. 2 shows a schematic cross section of a high-

† This paper was recommended for publication in revised form by Associate Editor Kyoung Doug Min

*Corresponding author. Tel.: +82 2 705 8635, Fax.: +82 2 712 0799
E-mail address: kj_myong@hotmail.com, kjmyong@chosun-c.ac.kr

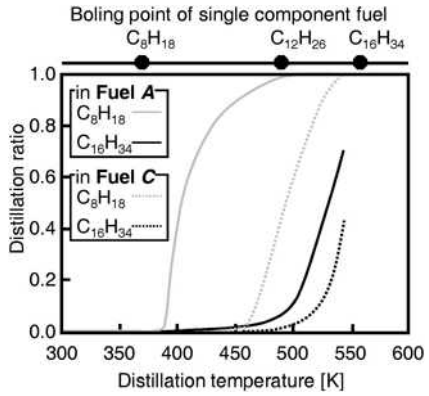

Fig. 1. Distillation curve of each component of multi-component fuel.

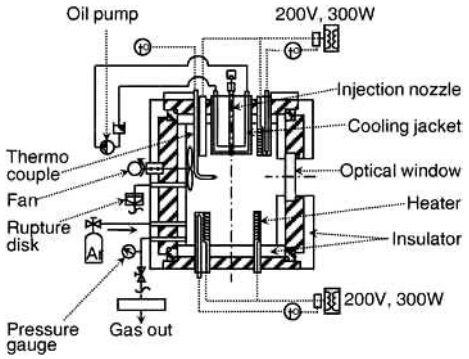

Fig. 2. Schematic cross-section of the constant volume vessel.

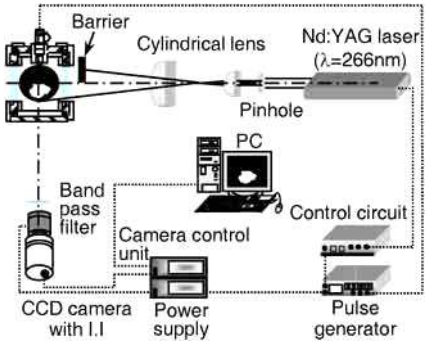

Fig. 3. Optical setup of laser induced fluorescence.

temperature and high-pressure constant-volume vessel [5]. Optical measurement can be possible through the three quartz windows, and the diameter of a window is 100mm. The allowable pressure of the constant-volume vessel is 3MPa, and fuel-spray injector is inserted into the cooling jacket set into the cool injector. Mixing fan, set in the left side of the vessel, works at 1000rpm to rapidly equilibrate ambient gas temperature before fuel injection. The rupture disk is ruptured when the vessel exceeds the allowable pressure, and internal gas is given off. Internal pressure and temperature are controlled by argon (Ar) gas and cartridge heaters set at upside and downside, respectively.

2.2 Optical setup

Fig. 3 shows the LIF imaging system. The second harmonic of the Nd-YAG laser at 266nm (power 18mJ/pulse after pinhole, pulse width: 8 ns, maximum frequency: 10Hz) was used as light source. Incident light, passed through the pinhole (ϕ=10mm), is turned into a beam of thickness 0.2mm through three cylindrical lenses (focus length f=40mm, f=320mm, f=1000mm), and is projected on the central axis of fuel jet. Pinhole was used to better the uniformity of the laser sheet. Incident light was partially excluded by setting a barrier in front of the constant-volume vessel to remove fluorescence and elastically scattered light due to droplets. The length of cut incident light was determined by the liquid phase length of MCF investigated previously [5, 6]. Liquid phase length becomes longer with time, and reaches quasi-state before spray stop. Fluorescence of fuel vapor is captured by using a CCD camera (Hamamatsu Photonics, Model C4742-95) with an image intensifier (Hamamatsu Photonics, Model C4078-01), and camera lens was a UV lens (Nikon: UV-Nikkor, f-105mm). An optical interference filter (wavelength=451.2mm, FWHM=6.5mm, rate of transmission=71.7%) was set in front of the image intensifier so that only fluorescence could be captured. Laser pulse is synchronized by one-shot trigger, and the trigger is transmitted by an injector and a CCD camera. An injector signal is delayed by pulse generator (Stanford research systems: Model DG535), and so fluorescence can be captured at another timing of arbitrary developing spray.

2.3 Experimental condition and fuel tested

Table 1 shows the experimental conditions. This study investigated the effects of injection condition, ambient gas one and the mass fraction of MCF on vapor-phase dispersion and mixture formation process. Miyagawa et al. [7] reported that at least three components should be compounded with each other so that real fuel can be simulated. Thus, we used three-component blended fuel in this study. Three

Table 1. Experimental conditions and mass fraction.

Test Fuel	Single component fuel (C_8H_{18}, $C_{12}H_{26}$, $C_{16}H_{34}$)	
	Multi-component fuel (Fuel ***A***, Fuel ***B***, Fuel **C**)	
Fuel Component	Mass Fraction of MCFs	
C_8H_{18} : $C_{12}H_{26}$: $C_{16}H_{34}$	6 : 3 : 1 **(Fuel *A*)**	
	1 : 1 : 1 **(Fuel *B*)**	
	1 : 3 : 6 **(Fuel *C*)**	
Injection Nozzle	Type : Hole nozzle DLL-p	
	Diameter of hole (d_n, mm)	0.2
	Length of hole (L_n, mm)	0.8
Amb. Temp. (T_{amb}, K)	700	
Fuel Tem. (T_{fuel}, K)	368	
Amb. Density (ρ_{amb}, kg/m^3)	15	
Inj. Pressure (P_{inj}, MPa)	42, 72, 112	
Amb. Gas	Ar	
Inj. Quantity (Q, mg)	12	

Injection duration t_{inj} (ms)

Fuel	P_{inj}=42 (MPa)	P_{inj}=72 (MPa)	P_{inj}=112 (MPa)
Fuel *A* (6 : 3 : 1)	2.31	1.82	1.57
Fuel *B* (1 : 1 : 1)	2.28	1.82	1.55
Fuel *C* (1 : 3 : 6)	2.26	1.81	1.51

single components were i-octane (C_8H_{18}), n-dodecane ($C_{12}H_{26}$) and n-hexadecane ($C_{16}H_{34}$), and were selected to be LO-B.P., MI-B.P. and HI-B.P. fuel, respectively. Fuels *A*, *B* and *C* were MCF in which single component fuels were mixed at the mixing fraction of 6:3:1, 1:1:1 and 1:3:6, respectively. The used injector was a hole-type nozzle (l/d=4). Fuel injection pressures were 42MPa, 72MPa and 112MPa, respectively, and ambient gas density was 15kg/m^3. Injection durations were evenly fixed to injection quantity 12mg in whole, and Argon (Ar) was used as ambient gas. Table 2 shows the properties of single-component fuel and MCF. These properties were calculated by NIST Thermo-Physical Properties of Hydrocarbon Mixture Database (SUPERTRAPP; version 1.0) [8].

2.4 Selection of dopant for fluorescence measurement on MCFs

Ordinarily, it was known that n-paraffin hydrocarbons are not excited, but Dec [9] reported that impurities with n-paraffin ones are fluorescent. It is because the impurities such as aromatic components, of which boiling points are similar to each other, are distilled almost simultaneously. In case these impurities are overlapped with the fluorescence band spectrum of dopant, the fluorescence phenomenon is not clearly observed. Thus, a verification test was performed to seek for optimal dopant, and to apply the LIF method to MCF, in consideration of fluorescence spectrum and concentration quenching.

Fig. 4 shows the optical setup used for the verification test. The fourth harmonic of an Nd-YAG laser at 266nm removes other wavelengths excluding 266nm by three dichroic mirrors, and is projected onto the quartz-glass cell containing sample. The fluorescence from sample is detected by fiber probe set at right angle to incident direction of laser and is stored to a photonic multi-channel analyzer (PMA C8808).

Fig. 5 shows the fluorescence wavelengths of fuel

Table 2. Fuel properties for single- and multi-component fuels.

Single component fuel	C_8H_{18}	$C_{12}H_{26}$	$C_{16}H_{34}$
Boiling point (T_b, K)	372	489	560
Density (293K)[a]	692	759	795
Viscosity (293K)[a]	508	1,542	3,394
Specific heat (293K)[a]	2.032	2.045	1.981
Latent heat of vaporization[b],	305.4	360.02	358.34
Latent heat of vaporization[b],	272	256.63	227.43
Diffusivity (293K)[b]	0.059	0.047	0.040
Molecular weight	114	170	226
Multi-component fuel	**Fuel *A***	**Fuel *B***	**Fuel *C***
Density (293K)[a] (ρ, kg/m^3)	722	748	773
Viscosity (293K)[a] (μ_l, μPa·s)	825	1,265	2,061
Specific heat (293K)[a]	2.036	2.027	2.010

[a] Calculation by the NIST Thermo-physical Properties of a Hydrocarbon Mixture Database (SUPERTRAPP) version a1.0, National Institute of Standards and Technology, 1992
[b] Bruce E. Poling, et al., "The properties of gases and liquids"

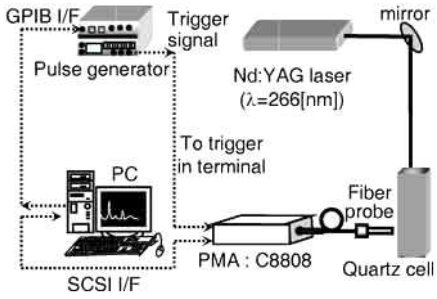

Fig. 4. Optical setup of measurement of fluorescent spectra.

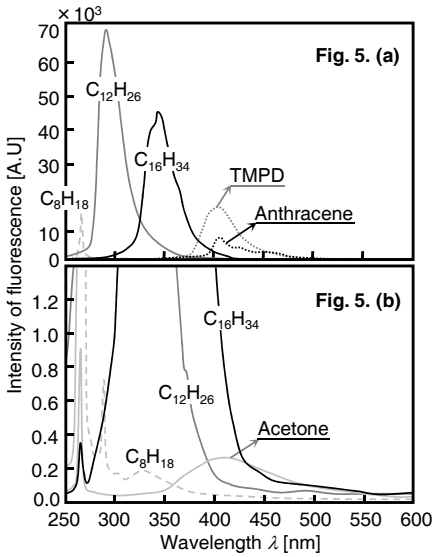

Fig. 5. Fluorescent wavelength of fuel and dopant (TMPD, anthracene and acetone).

and dopant. As shown in Fig. 5(a), the fluorescences of C_8H_{18}, $C_{12}H_{26}$ and $C_{16}H_{34}$, single-component fuels, have wide wavelengths from 270nm to 400nm due to impurities. For that reason, in case the dopant of which fluorescence intensity is higher than impurities is not selected in fluorescence wavelength over 400nm, the fluorescence is impossible to be separated from impurities and vapor-phase distribution of fuel is difficult to measure. TMPD and anthracene satisfy that condition, and fluorescence spectra from fuel (impurity) and dopant can be separately captured by using an interference filter. However, acetone, a dopant of LO-B.P. component, is impossible to show in Fig. 5 (a) because its intensity is very low as compared with other fuel (impurity) and dopant, and so was enlarged as in Fig. 5 (b). As shown in this figure, the fluorescence intensity of acetone is very low and its central wavelength is different from n-hexadecane, but the fluorescence bands accord with each other. As its fluorescence band is also mostly overlapped with those of n-dodecane, those are difficult to separate though an interference filter is used. But the fluorescence of acetone and i-octane (impurity) can be separated and measured because the intensity of i-octane is weak over 400nm. Thus, acetone was added to single component, not multi component, and its vapor-phase distribution was measured. And on the basis of those results, spatial vapor-phase distribution was estimated regarding the LO-B.P. component of

Table 3. Properties and fluorescence wavelength of fuel and dopant.

Fuel/ dopant	Molecular Weight	B.P. (K)	Diffusivity (cm^2/s)	Wave length *l* [nm]
C_8H_{18}	114.23	372	0.059	287
$C_{12}H_{26}$	170.33	489	0.047	290
$C_{16}H_{34}$	226.44	560	0.040	340
Acetone	58.08	330	0.098	417
TMPD	164	533	0.051	400
Anthracene	178.23	613	0.047	407

Table 4. Laser induced fluorescence (LIF) system of fuels tested.

Dopant	Fuel	Mixing ratio (Fuel/Doant)	Wavelength *l* (nm)
Acetone	C_8H_{18}	93.0/7.0 (vol. %)	451.2
TMPD	$C_{12}H_{26}$ ($C_{12}H_{26}$ in **Fuel *A*, *B*, *C)***	99.07/0.03 (mass %)	451.2
Anthracene	$C_{16}H_{34}$ ($C_{16}H_{34}$ in **Fuel *A*, *B*, *C)***	99.05/0.05 (mass %)	451.2

※ Fluorescence wavelength (451.2 nm) is central one of interference filter

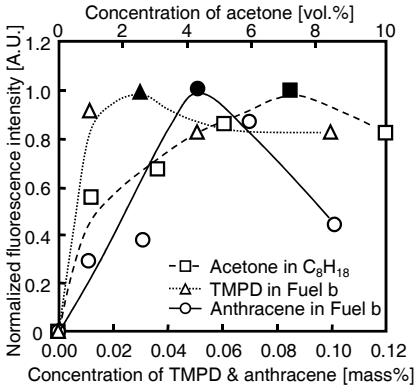

Fig. 6. Change in concentration of acetone, TMPD and anthracene.

MCF. In this study, TMPD and anthracene were used as tracers to MI-B.P. and HI-B.P. component within MCF, when acetone was used as the tracer to LO-B.P. one (i-octane single component) and fuel vapor-phase was measured.

As shown in Fig.6, fluorescence intensity was verified regarding the mixing concentration of dopant. TMPD was verified only to Fuel *B* because the results of anthracene were similar to each other for all MCFs

(Fuel *A*, *B* and *C*). The fluorescence intensity of acetone resulted from single-component fuel (i-octane). When mixing concentration is beyond an arbitrary mixing rate, its intensity becomes low due to concentration quenching. On that account, the concentration that indicates maximum intensity was selected to be the optimal mixing concentration of dopant.

Table 3 shows the properties and fluorescence wavelengths of single component fuel and dopant, and Table 4 shows the mixing ratio (fuel/dopant) and fluorescence wavelength of dopant which means the central one of the interference filter.

3. Results and discussion

3.1 Spatial vapor-phase distribution for single-component fuel

Fig. 7 shows the fluorescence images of TMPD and anthracene measured under same conditions. Fluctuation of fluorescence image is shown in each dopant to some degree, but it was not considered as there was no remarkable difference in fluorescence characteristic.

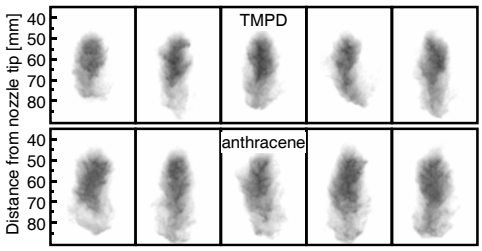

Fig. 7. Fluorescence images of TMPD and anthracene on the same conditions with **Fuel *B*** (t/t_{inj}=1.5, P_{inj}=72MPa).

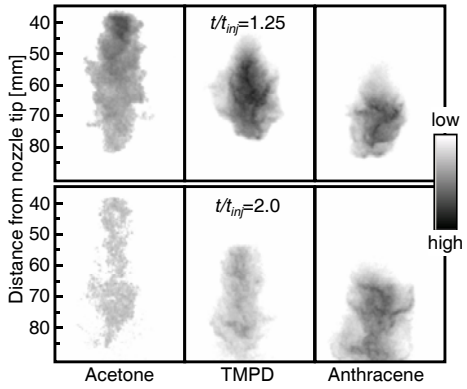

Fig. 8. Fluorescence image of acetone, TMPD and anthracene in single-component fuels (P_{inj}=42MPa).

Fig. 8 shows vapor-phase distribution of each dopant in single-component fuel. Injection pressure is 42MPa, dimensionless times (t/t_{inj}) are 1.25 and 2.0. When t/t_{inj} is 1.25, the acetonic vapor that corresponds to LO-B.P. component shows a homogeneous distribution over the spray downstream from 50mm to 80mm. In the case of the TMPD and anthracene that corresponds to MI-B.P. and HI-B.P. component, high-concentration vapor-phase is distributed over 50mm~75mm and 60mm~80mm, respectively. I-octane, an LO-B.P. component, is evaporated quickly by entrainment of high temperature surrounding gas at spray upstream because of its low latent heat of vaporization, and then vapor-phase is fast dispersed toward a radial direction with developing spray so that lean and homogeneous vapor-phase are distributed at spray midstream and downstream. MI-B.P. and HI-B.P. component, that is, n-dodecane and n-hexadecane, are slow in vaporizing due to high boiling point (high latent heat of vaporization), and high-concentration vapor phase is observed even after 80mm and its distribution is heterogeneous. When t/t_{inj} is 2.0, vapor-phases of acetone and TMPD become lean with time, and so the areas of these vapors get narrow. On the other hand, in the case of anthracene, high-concentration vapor is observed even when t/t_{inj} is 2.0 as well as vapor-phase is distributed over a wide area.

3.2 Spatial vapor-phase distribution of each component in MCF

As stated above, it was difficult to separately detect acetone from MCF spray, and so TMPD and anthracene were just captured.

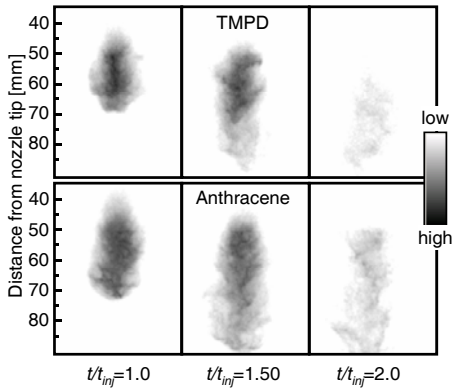

Fig. 9. Fluorescence image of TMPD and anthracene in **Fuel *B*** (P_{inj}=72MPa).

Fig. 9 shows the vapor-phase distributions of TMPD and anthracene regarding Fuel *B*. Injection pressure is 72 MPa and dimensionless times (t/t_{inj}) are 1.0, 1.5 and 2.0. In the case of Fuel *B*, each component is mixed at a ratio of 1:1:1, and i-octane, n-dodecane and n-hexadecane are of the same quantity nearly. The vapor-phase distribution of anthracene is wider than that of TMPD. When t/t_{inj} is 1.5, the vapor phase of anthracene is distributed between 75mm and 90mm and high concentration is formed at the downstream as compared with TMPD. When t/t_{inj} is 2.0, compared to anthracene, the evaporation and dispersion of TMPD rapidly progress. In this wise, the evaporation speeds of n-dodecane (MI-B.P. component) and n-hexadecane (HI-B.P. component) are different from each other, and so stratified distribution will be formed.

Fig. 10 shows the vapor-phase distribution of TMPD regarding Fuel *A*, *B* and *C*. Because n-dodecane in Fuels *A*, *B* and *C* is of the same quantity nearly, the TMPD is also of the same mass. On that score, those fuels begin to vaporize with time and fuel vapor is dispersed. Even if TMPD included in those fuels is of the same mass, the evaporation process is different from each other. As shown in Fig. 1, the distillation curve of each component in Fuel *A* is shifted to a low boiling point compared to that of Fuel *C* because Fuel *A* abundantly contains i-octane (LO-B.P. component) so that TMPD in Fuel *A* is rapidly evaporated and dispersed, and so vapor-phase concentration becomes lower as compared with Fuel *C*. It is thought that evaporation is early activated because of promotion of atomization and surrounding gas entrainment due to abundant LO-B.P. component. Likewise, evaporation and dispersion become slow in the order of Fuel *B* and *C*. In particular, the evaporation of n-dodecane (MI-B.P. component) in Fuel *C* is delayed because it contains n-hexadecane (HI-B.P. component) in abundance. From this result, it is found that the mixing ratio dominates the evaporation process of each component in MCF. That is, it can be seen that the evaporation and dispersion process of MI- and HI-B.P. component in MCF can be promoted by increasing the mixing ratio of the LO-B.P.

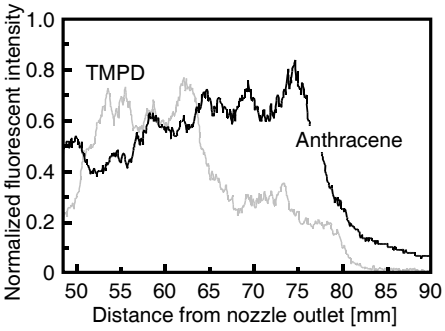

Fig. 11. Fluorescence intensities of TMPD and Anthracene on the central axis in **Fuel *B*** (P_{inj}=42MPa, t/t_{inj}=1.5).

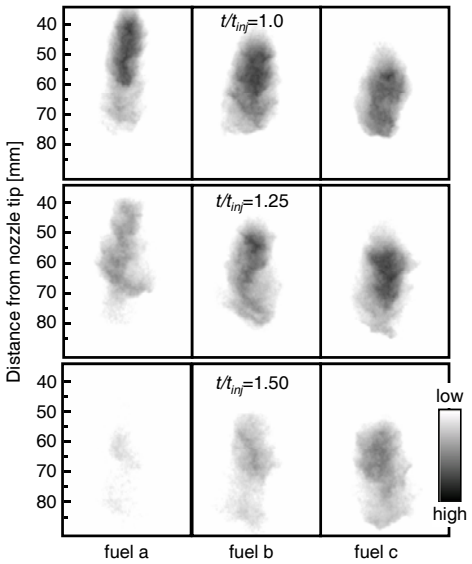

Fig. 10. Fluorescence image of TMPD in multi-component fuel (P_{inj}=112MPa).

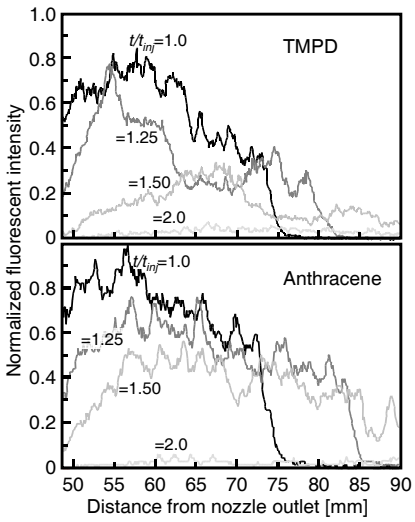

Fig. 12. Fluorescence intensities of TMPD and Anthracene on the central axis with time after injection stop in **Fuel *B*** (P_{inj}=112MPa).

3.3 Change in vapor-phase dispersion with time

Fig. 11 and Fig. 12 show how the intensity on the central spray axis changes. The maximum intensities of TMPD and anthracene were normalized, respectively. Fig. 11 shows the intensities of TMPD and anthracene on the spray axis, regarding Fuel *B*, under the conditions that injection pressure and dimensionless time (t/t_{inj}) are 42MPa, 1.5, respectively. The spray-axis intensity of TMPD is the highest between 50 and 65mm, and the intensity of anthracene begins to get high around 55mm and indicates the highest value between 65 and 75mm. Thus, the high-concentration vapor-phase distributions of TMPD and anthracene are different from each other. As compared with TMPD (MI-B.P. component), anthracene (HI-B.P. component) is distributed at the spray downstream and forms a stratified distribution.

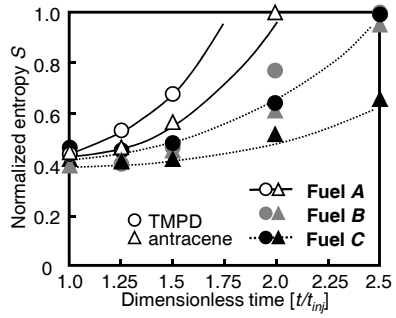

Fig. 13. Temporal change in entropies of TMPD and Antracene in different multi-component fuel (P_{inj}=72MPa).

Fig. 12 shows how the intensities of TMPD and anthracene change with time under the condition that injection pressure is 112MPa. When t/t_{inj} is 1.0, the intensities of TMPD and anthracene get lower with time. Evaporation is promoted with time, since injection starts, and a high-concentration vapor-phase is formed. And then vapor is shifted to the downstream and is widely dispersed by the vortex generated by the shear force to spray periphery. Thus, both dopants show lean vapor-phase distributions when t/t_{inj} is 2.0, and the intensity of the central axis approaches the zero point. In point of temporal change, the intensity of TMPD rapidly gets low as compared to that of anthracene. This is because TMPD is quick in evaporation and dispersion as compared to anthracene. It is found that the main distributional areas of each component of which boiling points are different from each other are different, that is, the components form stratified distributions. And a larger vapor phase is distributed around the spray axis in inverse proportion to dispersion speed, although time is elapsed after injection stops.

3.4 Assessment of vapor dispersion using entropy

As mentioned in 3.3, change in vapor-phase dispersion with time, dispersion is promoted as to the activation of evaporation; especially, vapor-phase distribution is lean at the spray downstream. Statistical entropy was herein worked out to quantitatively evaluate the degree of vapor-phase dispersion [10-12], and the dispersion process was analyzed under each

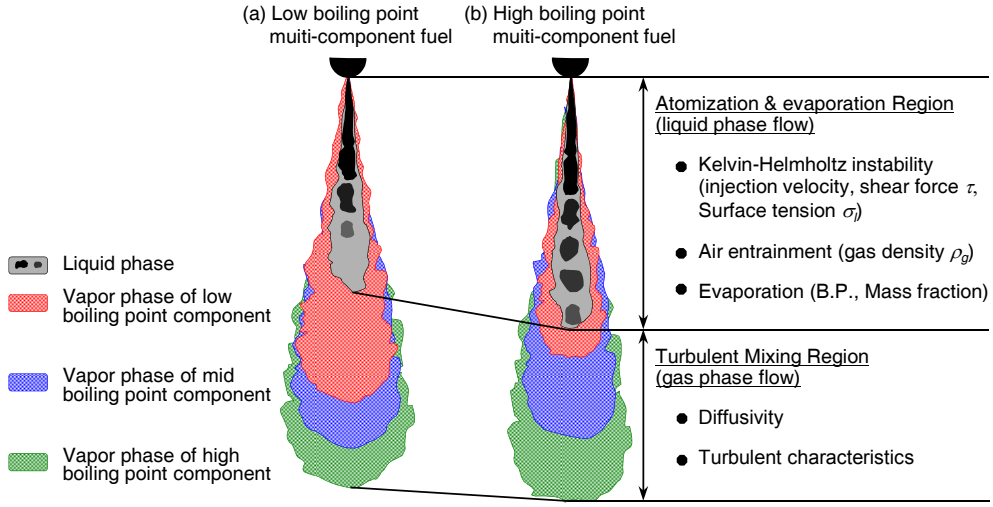

Fig. 14. Spatial distributions of liquid and vapor phase in evaporating multi-component fuel spray.

condition. Entropy shows a probability distribution, and its value tends to increase as fuel vapor is dispersed in the process that a mixture is formed. In this section, the case where all particles are homogeneously distributed on the image was normalized to '1', and the case where particles are cohered maximally was normalized to '0'. It means that fuel vapor is distributed more homogeneously as entropy approaches '1'.

Fig. 13 shows how the entropy of each dopant changes with time, regarding Fuels *A*, *B* and *C*, under the condition that injection pressure is 72MPa. The time taken to perfectly homogenize each component in Fuel *A* was shorter than that of Fuel *C*, and the mixture of each component in MCF gets more homogeneous in proportion as the boiling point gets lower. That phenomenon was also observed in other injection pressures, and the time got shorter in proportion as injection pressure increased. Thus, the mass fraction or mole fraction of LO-B.P. component in MCF exercises important influence on the mixture formation process, that is, homogeneous mixture formation. It is found that components and fractions of mixed fuel function as important factors in the evaporation, mixture formation and the dispersion process of MCF spray.

4. Conclusions

Fig. 14 shows a schematic diagram of the characteristic of spatial vapor-phase distribution of MCF spray. As reported in the previous study [13], the atomization behavior of MCF is remarkably influenced by the physical characteristics such as surrounding gas, aerodynamic interaction and fuel injection speed. Thus, the heterogeneous distributions of liquid-phase and liquid length are remarkably different in behavior as to the species and fraction of mixed fuel. Moreover, it is considered that the spatial distribution of vapor-phase is closely correlated with its homogeneity. This study concludes the following:

As evaporation of HI-B.P. component in MCF, which contains LO-B.P. one in abundance, is promoted by LO-B.P. one, its vapor-phase distribution tends to be homogeneous. It suggests that the evaporation process of MCF can be controlled physically.

In the case of the MCF that contains HI-B.P. component in abundance, the distribution of fuel vapor is apt to be stratified as well as UHC (unburned hydrocarbon) has a high possibility that its emission will increase.

In the case of the MCF containing LO-B.P. component in abundance, the mixture is rapidly dispersed as compared to the MCF that abundantly contains HI-B.P. component.

The heterogeneity of a locally rich mixture is improved by adding LO-B.P. component.

References

[1] J. Senda et al., Quantifying fuel concentration of diesel spray using planar laser Induced Exciplex fluorescence (PLIEF) method, Quantifying vapor phase concentration-1st report, *The Japan Society of Mechanical Engineering Series B* 63 (607) (1997) 322-327.

[2] J. Abraham and V. Magi, A model for multicomponent droplet vaporization in sprays, *SAE Paper* 980511 (1998).

[3] J. Senda and H. Fujimoto, Multi-component fuel consideration for spray evaporation field and spray-wall interaction, *SAE Paper* 2001-01-1071 (2001).

[4] J. Senda, T. Higaki, Y. Sagane and H. Fujimoto, Modeling and measurement on evaporation process of multi-component fuel, *SAE Paper* 2000-01-0280 (2000).

[5] K. J. Myong, M. Arai, H. Suzuki, S. Jiro and H. Fujimoto, Vaporization characteristics and liquid-phase penetration for multi-component fuels, *SAE Paper* 2004-01-0529 (2004).

[6] K. J. Myong, S. Hirotaka, S. Jiro and H. Fujimoto, Spray inner structure of evaporating multi-component fuel, *Fuel* 85 (17-18) (2006) 2632-2639.

[7] H. Miyagawa, M. Nagaoka, K. Ohsawa and T. Yamada, Spray vaporization model for multi-component gasoline, *JSAE* 19 (4) (1998) 299-304.

[8] *NIST thermo-physical properties of hydrocarbon mixture database (SUPERTRAPP) version 1.0*, National Institute of Standards and Technology (1992).

[9] J. E. Dec, A conceptual model of DI diesel combustion based on laser-sheet imaging, *SAE Paper* 970873 (1997).

[10] K. Ikeda, *Statistical Thermodynamics*, Kyowa Publishing (1992).

[11] I. Nakagawa, *An introduction to molecular statistical mechanics*. Tokyo chemical Dojin Publishing (1974).

[12] Y. Ryo et al., Micro structure and air entrainment of diffusion within spray, *16th Internal Combustion Engine Symposium* (2000) 235-240.

[13] K. J. Myong, S. Hirotaka, S. Jiro and H. Fujimoto, Spray inner structure of evaporating multi-component fuel, *Fuel* 87 (2) (2008) 202-210.

Jun-Kyu Yoon received his B.S., M.S. and Ph.D degrees from the department of Mechanical Engineering, Chosun University, Kyunghee University and Myongji University in 1981, 1987 and 2001, respectively. He worked at Hyundai Motors and Asia Motors Company from 1985 to 1996. He has worked for department of mechanical and automotive engineering at Kyungwon University and is currently a professor. His research interests include internal combustion engineering, heat transfer analysis, air conditioning and refrigeration.

Kwang-Jae Myong received his B.S. in Automobile Engineering from Kookmin University, KOREA, in 1998. He then received his M.S. degree from Chonnam National University, KOREA, in 2000 and Ph.D. degree from Doshisha University, JAPAN, in 2005. He worked at National Traffic Safety & Environment Laboratory, JAPAN, from 2005 to 2008. Dr. Myong is currently a Professor at the department of Automobiles at Chosun College of Science & Technology in Gwang-ju, Korea. His research interests include internal combustion engines and HEVs.

J. Senda received his B.S., M.S. and Ph.D. degrees from Doshisha University, JAPAN, in 1978, 1980 and 1985, respectively. Dr. Senda is currently a Professor at the department of Mechanical Engineering at Doshisha University in Kyoto, JAPAN. His research interests include internal combustion engines, sprays and combustion.

H. Fujimoto received his B.S., M.S. and Ph.D. degrees from Keio University, JAPAN, in 1964, 1966 and 1974, respectively. Dr. Fujimoto is currently a Professor at the department of Mechanical Engineering at Doshisha University in Kyoto, JAPAN. His research interests include internal combustion engines, sprays and combustion.